PAPER

Check for updates

Host–guest modes and supramolecular frameworks of complexes of tetramethyl cucurbit[6]uril with 4-chloroaniline and 4,4′-diaminostilbene†

Ye Meng, Weiwei Zhao, Jun Zheng, Daofa Jiang, Jie Gao, Yanmei Jin and Peihua Ma (ID) *

Since the first reportal on decamethylcucurbit[5]uril (Me$_{10}$Q[5]) in 1992, substituted cucurbit[*n*]urils have attracted considerable research interest. In this study, the host–guest modes between the tetramethyl cucurbit[6]uril (TMeQ[6]) as a host and 4-chloroaniline and 4,4′-diaminostilbene (**G1** and **G2**) as guests were investigated by single-crystal X-ray diffraction, NMR, ITC, UV-Vis spectrum, and MALDI-TOF mass spectrometry analyses. The experimental results showed that TMeQ[6] formed a 1 : 1 inclusion compound with **G1**, and the carbonyl portal of TMeQ[6] formed a 1 : 1 self-assembly with **G2**. Further, multi-dimensional supramolecular frameworks were formed driven by weak interaction forces in the system (hydrogen bonding, C–H⋯π interactions, ion–dipole interactions, and dipole–dipole interactions).

1. Introduction

Various porous materials, namely, inorganic porous materials[1,2] (such as molecular sieves), organic–inorganic hybrid porous materials[3–5] (such as metal–organic frameworks, MOFs), and porous organic framework (POF) materials[6,7] have been developed. These porous materials have been widely used in adsorption, heterogeneous catalysis, and ion exchange processes.[8–10] Interestingly, in recent years, the use of weak forces as the driving force to construct supramolecular frameworks has been explored,[11,12] so the selection of suitable construction units has also become crucial. Cucurbit[*n*]uril is a fourth-generation supramolecular macrocyclic compound after crown ether, cyclodextrin, and calixarene; there are two main types: ordinary cucurbit[*n*]urils[13–18] and modified cucurbit[*n*]urils (decamethylcucurbit[5]uril, cyclopentyl-modified cucurbit[*n*]urils and so on).[19–24] Their structure has a hydrophobic cavity, two carbonyl portals, and an outer surface. The charge distribution in cucurbit[*n*]uril itself is not uniform, which makes cucurbit[*n*]uril a permanent dipole[25] (the cavity of the cucurbit[*n*]uril has an electrically neutral potential, the outer surface has a positive potential, and the carbonyl portal shows a negative potential). This is conducive to the study of the host–guest chemistry[26–30] and coordination chemistry[31–35] of the cucurbit[*n*]uril, and to the construction of good reversible supramolecular organic frameworks[36,37] (SOFs).

Based on A–H⋯B (A and B are oxygen, nitrogen or fluorine) hydrogen bond theory.[38] There was ion–dipole interaction between [ZnCl$_4$]$^{2-}$ and [CdCl$_4$]$^{2-}$ anions and positive potential outer surface of cucurbit[*n*]urils, which makes them conducive to the construction of self-assembly complexes based on cucurbit[*n*]uril, so considered to be known to function as effective structure directing agents.[39] In this work, [ZnCl$_4$]$^{2-}$ (formed from ZnCl$_2$ in an aqueous HCl solution) was used as structure directing agents, TMeQ[6]-based SOFs, namely, C$_{92}$H$_{110}$Cl$_{17}$N$_{50}$O$_{28}$Zn$_4$ (**1**) and C$_{68}$H$_{76}$Cl$_8$N$_{28}$O$_{12}$Zn$_2$ (**2**) were constructed by the supramolecular collaborative assembly. The driving force of complexes **1** and **2** was studied through single-crystal X-ray diffraction analysis, and the host–guest interaction between TMeQ[6] and guest molecules was studied through NMR, ITC, UV-Vis spectrum and MALDI-TOF mass spectrometry analyses. The experimental results showed that TMeQ[6]-based host–guest SOFs are promising for several applications, *e.g.*, in selective adsorption, heterogeneous catalysis, and ion exchange (Scheme 1).

2. Experimental

2.1 Experimental reagents

All the reagents were purchased from Aladdin Industrial Corporation (AR, Shanghai, China). TMeQ[6] was synthesized according to the method reportaled in a previous paper.[40]
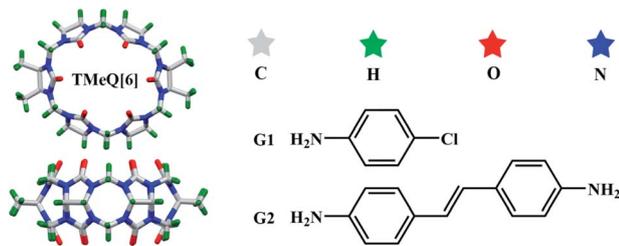
2.2 Synthesis of the complexes

TMeQ[6] (10 mg, 9.51 μmol) and **G1** (2.55 mg, 20 μmol) were placed in a crystal bottle and 3 mol L^{-1} hydrochloric acid (5 mL) was added;

Scheme 1   TMeQ[6] and guest molecules used in this study.

the mixture was heated until dissolution. Then, a small amount of the inducing agent $ZnCl_2$ was added, and the solution was heated and stirred for 5–10 min in a water bath at 35 °C. Finally, the solution was allowed to stand at room temperature for 7–10 days to obtain single crystals of complex **1** (35% yield). Complex **2** was synthesized (28% yield) in the same manner as complex **1**.

2.3   Crystal structure determination

A crystal with the appropriate size and transparency was selected and fixed on a glass probe with petroleum jelly. A Bruker Smart Apex II single-crystal X-ray diffractometer, with Mo-K$_\alpha$ radiation ($\lambda = 0.071073$ nm), was used for the characterization. The SHELX-97 (ref. 41) program packages were used for data refinement by the full-matrix least-squares method, and the SQUEEZE routine of the PLATON program was used to process solvent molecules in the crystal. The X-ray crystallographic data for structures reportaled in this study have been deposited in the Cambridge Crystallographic Data Center under accession numbers CCDC: 2039065 (**1**) and 2039066 (**2**).† The crystal parameters, data acquisition conditions, and parameters of the complexes **1** and **2** are listed in Table 1.

Table 1   Crystallographic data for complexes 1 and 2[a]

	1	2
Empirical formula	$C_{92}H_{110}Cl_{17}N_{50}O_{28}Zn_4$	$C_{68}H_{76}Cl_8N_{28}O_{12}Zn_2$
Formula weight	3228.42	1891.90
Crystal system	Triclinic	Triclinic
Space group	$P\bar{1}$	$P\bar{1}$
a [Å]	18.070(3)	11.664(5)
b [Å]	21.050(3)	14.379(7)
c [Å]	21.095(5)	15.558(7)
α [°]	105.503(9)	101.417(14)
β [°]	104.705(8)	100.443(15)
γ [°]	104.621(5)	107.344(14)
V [Å³]	7023(2)	2359.4(19)
Z	2	1
$D_{calcd.}$ [g cm^{-3}]	1.527	1.331
T [K]	273.15	273.15
μ [mm^{-1}]	1.082	0.802
Parameters	1730	536
R_{int}	0.0444	0.1199
R [$I > 2\sigma(I)$][a]	0.0531	0.1182
wR [$I > 2\sigma(I)$][b]	0.1542	0.3377
R (all data)	0.0783	0.2050
wR (all data)	0.1702	0.3755
GOF on F^2	1.051	1.110

[a] Note: [a] Conventional R on $Fhkl$: $\sum \|F_0| - |F_c\|/\sum|F_0|$; [b] weighted R on $|Fhkl|^2$: $\sum[w(F_0{}^2 - F_c{}^2)^2]/\sum[w(F_0{}^2)^2]^{1/2}$.

2.4   Determination by ^{1}H NMR

G1, **G2**, and TMeQ[6] were each dissolved in neutral D_2O. The guest solution concentration was fixed at 0.1 mM in all analyses. The TMeQ[6] solution was added dropwise until it was in excess of the guest solution, and the ^{1}H NMR spectra were recorded at appropriate intervals using a JEOL JNM-ECZ400s spectrometer at 25 °C. D_2O was used as a field-frequency lock, and the observed chemical shifts are reportaled in parts per million (ppm) relative to D_2O as an internal standard ($\delta = 4.67$ ppm).

2.5   Determination by isothermal titration calorimetry

The neutral aqueous solution of TMeQ[6] (1.0×10^{-4} mol L^{-1}, 1.00 mL) was placed in the sample cell, and a 1.00×10^{-3} mol L^{-1} **G1** solution was drawn into a 250 mL syringe. The temperature was set at 25 °C, and the titration was conducted by adding 30 aliquots (8 μL) of the **G1** solution at intervals of 300 s. The same method was used for TMeQ[6] and **G2**. The thermodynamic parameters of each system were determined on a nano ITC isothermal calorimeter. After deleting the first one unwanted data points, the data were analyzed with Launch NanoAnalyze software using an independent model.

2.6   Determination by UV-Vis spectrum

The neutral aqueous solution of TMeQ[6] (1.0×10^{-4} mol L^{-1}) and **G1** (1.0×10^{-3} mol L^{-1}) were prepared as stock solutions, and the UV-Vis absorption spectrum of each substance was measured by the molar ratio. Add 300 μL of **G1** stock solution to eleven 10 mL volumetric bottles, then add corresponding volume of TMeQ[6] stock solution to these volumetric bottles, and maintain molar ratios of 0, 0.2, 0.4, 0.6, 0.8, 1.0, 1.2, 1.4, 1.6, 1.8 and 2.0 after volume determination with doubly-distilled water. The measurements were performed at room temperature with an UV-2700 external spectrometer. The same method was used for TMeQ[6] and **G2**.

2.7   Determination by mass spectrometry

The neutral aqueous solution of TMeQ[6] (1.0×10^{-4} mol L^{-1}) was prepared, and 1 mL was pipetted into a centrifuge tube. Then, 100 μL of the **G1** aqueous solution with a concentration of 1×10^{-3} mol L^{-1} was added. The solution was filtered into a chromatographic sample bottle using aqueous 0.22 μm syringe filters. Mass spectra were recorded on an Agilent 6545 Q-TOF mass spectrometer. The same method was used for TMeQ[6] and **G2**.

3.   Results and discussion

3.1   Description of the crystal structures of complexes 1 and 2

3.1.1   Description of the crystal structure of complex 1. Complex **1** exhibits the triclinic $P\bar{1}$ space group. As shown in Fig. 1a, TMeQ[6] and protonated 4-chloroaniline formed a 1 : 1 inclusion compound. In this system, hydrogen bonds are one of the main forces. N49 forms three hydrogen bonds with O2, O4, and O6, and N50 forms three hydrogen bonds with O16, O18, and O20; the N–H⋯O hydrogen bond length is 2.760–2.834 Å. In addition, hydrogen bonds form between O1 and O2 and
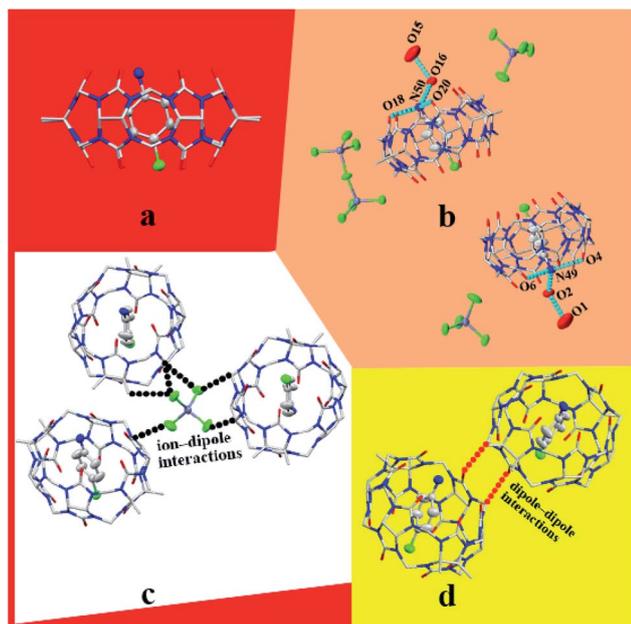
Fig. 1 Structure of complex **1**: (a) 1 : 1 inclusion compound of TMeQ [6] and **G1**, (b) hydrogen bond interaction, (c) ion–dipole interaction, and (d) dipole–dipole interaction.

between O15 and O16 (O2–H2A⋯O1 and O16–H16A⋯O15), with the bond lengths being 2.859 and 2.855 Å, respectively (Fig. 1b). One counterion $[ZnCl_4]^{2-}$ connects with three adjacent outer surfaces of TMeQ[6]s via ion–dipole interactions (Fig. 1c). A negatively potential TMeQ[6] portal is connected to another positively potential outer surface of TMeQ[6] by the dipole–dipole interaction (Fig. 1d). In summary, these weak interactions
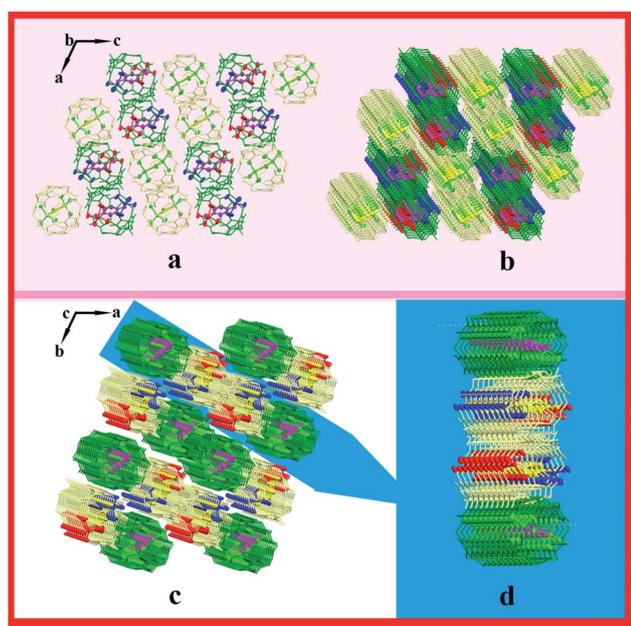
(hydrogen bonding, ion–dipole interaction, and dipole–dipole interaction) caused complex **1** to form an ordered multi-dimensional layered supramolecular framework (Fig. 2a–d).

3.1.2 Description of the crystal structure of complex 2. Complex **2** exhibits the triclinic $P\bar{1}$ space group. The asymmetric unit contains half of TMeQ[6], one counterion $[ZnCl_4]^{2-}$, and two half of protonated 4,4′-diaminostilbenes, as shown in Fig. 3a. Counterions $[ZnCl_4]^{2-}$ connects with adjacent TMeQ[6]s by ion–dipole interactions (Fig. 3b). In fact, protonated 4,4′-diaminostilbene also connects with the methylene hydrogen (–CH) and bridging "waist" methylene (–CH$_2$) of TMeQ[6]s by C–H⋯π interactions (Fig. 3c). Further, TMeQ[6] and protonated 4,4-diaminostilbene form a 1 : 1 assembly via hydrogen bonds, where N1 of protonated 4,4-diaminostilbene forms two hydrogen bonds with O1 and O2 of TMeQ[6], and N14 of protonated 4,4-diaminostilbene forms a hydrogen bond with Cl2 of counterions $[ZnCl_4]^{2-}$. These hydrogen bonds—i.e., N1–H1A⋯O1, N1–H1B⋯O2, and N14–H14A⋯Cl2—have bond lengths of 2.789, 2.734, and 3.277 Å, respectively (Fig. 3d). Hydrogen bonding, C–H⋯π, and ion–dipole interactions were the driving forces in the construction of the supramolecular assembly. As shown in Fig. 3e, the extension of supramolecular assembly at different angles can result in different shapes. By taking the angle of view along the b-axis as an example and by only considering the hydrogen bond between the portal of TMeQ[6] and 4,4′-diaminostilbene, a one-dimensional supramolecular chain is formed (Fig. 4a). Interestingly, when multiple forces coexist, 4,4′-diaminostilbene forms a "walled" supramolecular framework enclosing TMeQ[6]s, eventually forming the two-dimensional supramolecular framework (Fig. 4b) and the three-dimensional framework (Fig. 4c).
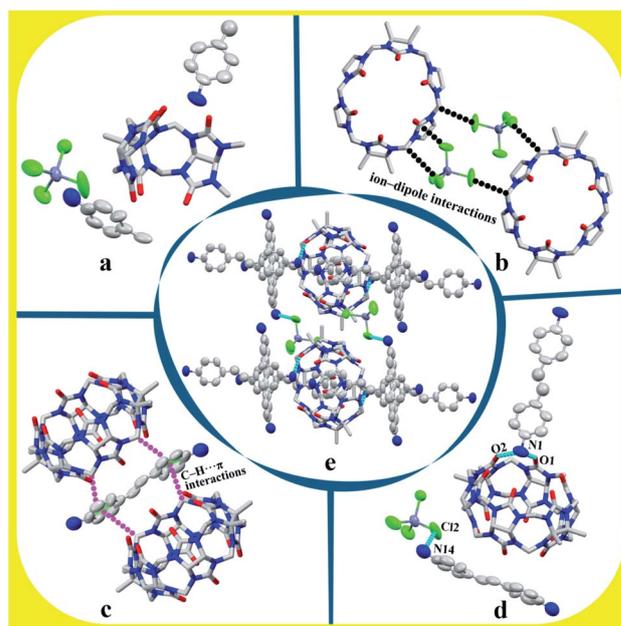

Fig. 2 Supramolecular framework of complex **1**: (a) two-dimensional framework structure viewed along the b-axis, (b and c) three-dimensional supramolecular framework structure viewed along b-axis and c-axis, respectively, and (d) three-dimensional layered framework.

Fig. 3 Structure of complex **2**: (a) asymmetric unit, (b) ion–dipole interaction, (c) C–H⋯π interaction, (d) hydrogen bond interaction, and (e) assembly of unit cell.
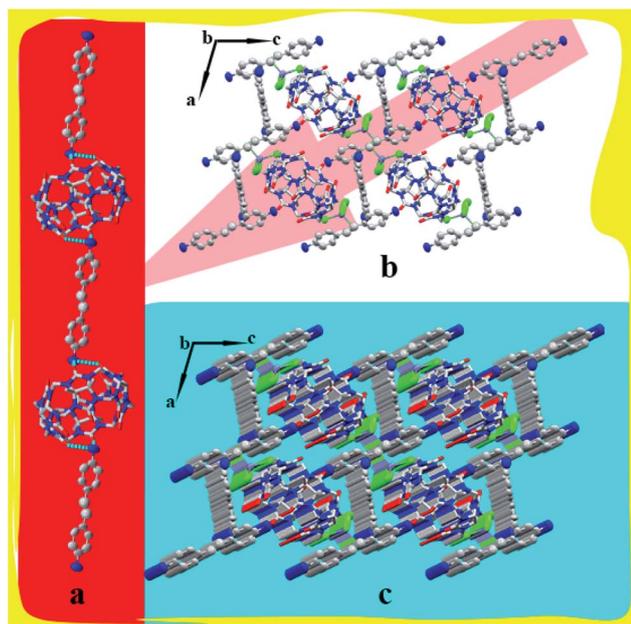
Fig. 4 Supramolecular framework of complex 1: (a) one-dimensional framework chain, (b) two-dimensional supramolecular framework structure viewed along *b*-axis, and (c) three-dimensional framework along *b*-axis.

3.2 ¹H NMR, ITC, UV-Vis spectrum, and MALDI-TOF mass spectrometric analysis of cucurbiturils and guests

3.2.1 ¹H NMR spectra of TMeQ[6] and guests. The cavity of TMeQ[6] has a shielding effect on proton signals, whereas outside of the portals, in the vicinity of the carbonyl oxygen atoms, the proton signals are subjected to a deshielding effect. Therefore, nuclear magnetic resonance (NMR) is one of the most commonly used techniques to investigate host–guest interactions. Fig. 5 and 6 show the ¹H NMR results of interactions of **G1** and **G2** with TMeQ[6] in D_2O, respectively.

Fig. 5a shows the ¹H NMR spectrum of **G1**; Fig. 5b, c, and d show the ¹H NMR spectra of TMeQ[6]–**G1** with an equivalent ratio of 0.51, 1.08, and 1.36, respectively; and Fig. 5e shows the
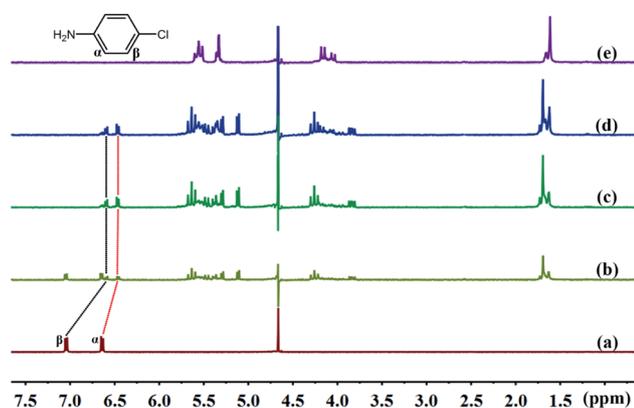

Fig. 5 Titration ¹H NMR spectra of G1 (0.1 mM) with (a) 0.00, (b) 0.51, (c) 1.08, and (d) 1.36 equiv. of TMeQ[6], and of (e) neat TMeQ[6].
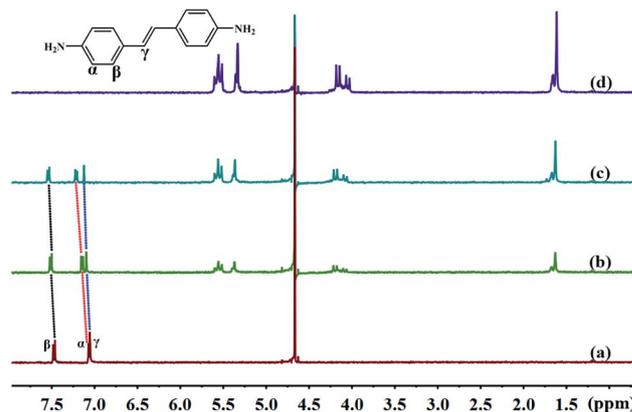

Fig. 6 Titration ¹H NMR spectra of G2 (0.1 mM) with (a) 0.00, (b) 0.71, and (c) 1.39 equiv. of TMeQ[6], and of (d) neat TMeQ[6].

¹H NMR spectrum of TMeQ[6]. When TMeQ[6] was added to the system, the chemical shift of H_α and H_β protons of **G1** moved upfield by about δ 0.175 and 0.449 ppm, respectively. This indicates that **G1** penetrated into the cavity of TMeQ[6] and was shielded by TMeQ[6]. Moreover, when TMeQ[6] was greater than 1 equiv., the chemical shift of protons H_α and H_β remained unchanged, indicating that TMeQ[6] and **G1** formed a 1 : 1 inclusion compound, and the existence of the amino group and Cl atom in **G1** resulted in the splitting of proton peaks of TMeQ[6].

Further, Fig. 6a shows the ¹H NMR spectrum of **G2**; Fig. 6b and c show the ¹H NMR spectra of TMeQ[6]–**G2** with an equivalent ratio of 0.71 and 1.39, respectively; and Fig. 6d shows the ¹H NMR spectrum of TMeQ[6]. When TMeQ[6] was added to the system, the chemical shifts of the protons H_α, H_β, and H_γ of the guest **G2** moved downfield, indicating that **G2** was at the portal of TMeQ[6] and was subject to the deshielding effect of TMeQ[6]. The proton peaks of TMeQ[6] did not split, indicating that the protons of TMeQ[6] were in a symmetrical environment. By comparing Fig. 6b and c, when the amount of TMeQ[6] increased, the protons H_α, H_β and H_γ of the guest **G2** moved up to the downfield, indicating that TMeQ[6] and **G2** was an unstable reversible dynamic interaction.[42]

3.2.2 Isothermal titration calorimetry. Isothermal titration calorimetry (ITC) experiments (Fig. 7) were performed to determine the thermodynamic parameters of the above two guests and TMeQ[6] in water, providing insight into the thermal
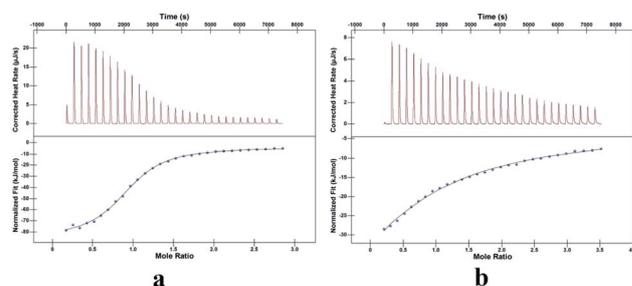

Fig. 7 Titration diagram of isothermal titration calorimetry: (a) TMeQ [6]@G1, (b) TMeQ[6]@G2.

Table 2 Thermodynamic parameters of the interactions of TMeQ[6] with **G1** and **G2**

Experiment	K_a (M^{-1})	ΔH (kJ mol^{-1})	$T\Delta S$ (kJ mol^{-1})	ΔG
G1·TMeQ[6]	1.484×10^5	−80.89	−51.37	−29.52
G2·TMeQ[6]	5.194×10^3	−100.00	−78.79	−21.21

stability and driving force of the interactions. The enthalpies and entropies of the interactions of the two guests and TMeQ[6] are both negative (Table 2). From the contributions of these two thermodynamic parameters to the Gibbs free energy ($\Delta G = -RT \ln K_a = \Delta H - T\Delta S$), it can be seen that the two systems are enthalpy-driven, and the driving force is determined by the hydrogen bond interaction and the hydrophobic effect. By comparing the binding constants of **G1**·TMeQ[6] and **G2**·TMeQ[6], the stability of **G1** entering the cavity of TMeQ[6] is greater than that of **G2** at the portals of TMeQ[6]. **G2**·TMeQ[6] has a weak binding affinity, resulting in a reversible dynamic interaction of **G2**·TMeQ[6] (Table 2).

3.2.3 UV-Vis spectrum analysis. The binding behaviors of TMeQ[6]@**G1** and TMeQ[6]@**G2** were studied by employing UV-Vis absorption in deionized water (Fig. 8). The wavelengths of the one strong absorption peak for **G1** was observed at 238 nm, and TMeQ[6] exhibited no absorption at these wavelengths. The absorbance of **G1** shows a gradually downward trend upon increasing the ratio of n(TMeQ[6])/n(**G1**). When the ratio of n(TMeQ[6])/n(**G1**) reaches 1, the absorbance becomes stable as the ratio increases. Therefore, the absorbance (A) *vs.* the molar ratio of the TMeQ[6] and **G1** {n(TMeQ[6])/n(**G1**)} data can be fitted to a 1 : 1 binding (Fig. 8a). In addition, the wavelengths of the one strong absorption peak for **G2** was observed at 306 nm, and TMeQ[6] exhibited no absorption at these wavelengths. The absorbance of **G2** shows a gradually downward trend upon increasing the ratio of n(TMeQ[6])/n(**G2**). According to the tangent intersection, the absorbance (A) *vs.* the molar ratio of the TMeQ[6] and **G2** {n(TMeQ[6])/n(**G2**)} data can be fitted to a 1 : 1 binding (Fig. 8b).

3.2.4 Mass spectrometry. In order to further investigate the host–guest interaction modes, as shown in Fig. 9, matrix-assisted laser desorption/ionization time-of-flight (MALDI-TOF) mass spectrometry was used to characterize the complex structures. The molecular ion peaks are visible at m/z 1180.3840 and 1263.4626, and these could correspond to [TMeQ[6] + **G1** + H]$^+$ and [TMeQ[6] + **G2** + H]$^+$, respectively (calculated m/z values
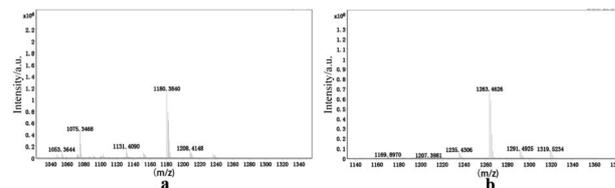

Fig. 9 Mass spectrometry of (a) TMeQ[6]@**G1**, and (b) TMeQ[6]@**G2**.

were 1180.3832 and 1263.4811, respectively). Therefore, TMeQ[6] and guests interacted at a ratio of 1 : 1, which is consistent with the above analysis results.

4. Conclusions

In this study, the interaction modes of TMeQ[6] with **G1** and **G2** were investigated by performing single-crystal X-ray diffraction, NMR, ITC, UV-Vis spectrum, and MALDI-TOF mass spectrometry analyses. The experimental results showed that TMeQ[6] and **G1** formed a 1 : 1 inclusion complex, and the carbonyl portal of TMeQ[6] formed a 1 : 1 self-assembly with **G2**. The single crystal structures of complexes **1** and **2** exhibited the ion–dipole interaction, dipole–dipole interaction, C–H···π interaction, and hydrogen bonds. These weak interaction forces caused complexes **1** and **2** to form ordered multi-dimensional supramolecular frameworks. They are expected to have a wide range of applications in nanotechnology, molecular sieves, sensors, gas adsorption and separation, ion or molecular transportal, and heterogeneous catalysis.

Conflicts of interest

There are no conflicts to declare.

Acknowledgements

Notes and references

1 J. M. Thiebaut and C. Akyel, *IEEE Trans. Instrum. Meas.*, 1988, **37**(1), 114–120.
2 L. Zhao, R. Y. Ma and X. L. Meng, *Adv. Mater. Res.*, 2012, **450**, 1419–1424.
3 X. Zhao, D. Liang and S. Liu, *Inorg. Chem.*, 2008, **47**(16), 7133–7138.
4 Y. Cu, Y. Yue and G. Qian, *Chem. Rev.*, 2012, **112**(2), 1126–1162.
5 J. R. Li, R. Kuppler and H. C. Zhou, *J. Cheminf.*, 2009, **38**(5), 1477–1504.
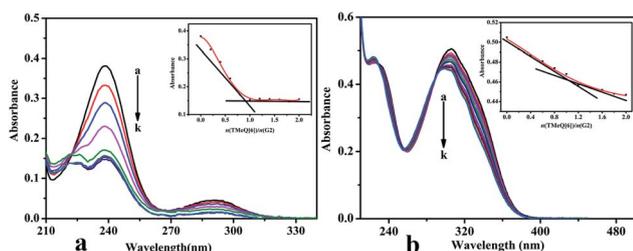6 H. Furukawa and O. M. Yagh, *J. Am. Chem. Soc.*, 2009, **131**(25), 8875–8883.

Fig. 8 UV-Vis spectrum of (a) TMeQ[6]@**G1**, and (b) TMeQ[6]@**G2**.

7 F. Beuerle and B. Gole, *Angew. Chem., Int. Ed.*, 2018, **57**, 4850–4878.

8 C. Shuai, Z. Mo and X. Niu, *J. Alloys Compd.*, 2020, **847**, 156514.

9 Y. Su, Z. Li and H. Zhou, *Chem. Eng. J.*, 2020, **402**, 126205.

10 C. H. Lin, Z. F. Zao and Z. W. Lei, *Spectrochim. Acta, Part A*, 2020, **242**, 118739.

11 W. Yang, A. Greenaway, X. Lin, R. Matsuda, A. J. Blake, C. Wilson, W. Lewis, P. Hubberstey, S. Kitagawa and M. Schröder, *J. Am. Chem. Soc.*, 2010, **132**, 14457–14469.

12 J. Tian, H. Wang, D. W. Zhang, Y. Liu and Z. T. Li, *Natl. Sci. Rev.*, 2017, **4**, 426–436.

13 W. A. Freeman, W. L. Mock and N. Y. Shih, *J. Am. Chem. Soc.*, 1981, **103**(24), 7367–7368.

14 K. Kim, N. Selvapalam and D. H. Oh, *J. Inclusion Phenom. Macrocyclic Chem.*, 2004, **50**(1–2), 31–36.

15 A. Day, A. P. Arnold, R. J. Blanch and B. Sunshall, *J. Org. Chem.*, 2001, **66**(24), 8094–8100.

16 A. I. Day, R. J. Blanch, A. P. Arnold and G. R. Lewis, *Angew. Chem.*, 2002, **41**, 275–277.

17 S. Liu, P. Y. Zavalij and L. Isaacs, *J. Am. Chem. Soc.*, 2005, **127**(48), 16798–16799.

18 X. J. Cheng, L. L. Liang, K. Chen, N. N. Ji, X. Xiao, J. X. Zhang, Y. Q. Zhang, S. F. Xue, Q. J. Zhu, X. L. Ni and Z. Tao, *Angew. Chem., Int. Ed.*, 2013, **52**(28), 7252–7255.

19 A. Flinn, G. C. Hough, J. F. Stoddart and D. J. Williams, *Angew. Chem., Int. Ed.*, 1992, **31**(11), 1475–1477.

20 J. H. Zhao, H. J. Kim, J. H. Oh, S. Y. Kim, J. W. Lee, S. Sakamoto, K. Yamaguchi and K. Kim, *Angew. Chem.*, 2001, **113**(22), 4363–4365.

21 F. Wu, L. H. Wu, X. Xiao, Y. Q. Zhang, S. F. Xue, Z. Tao and A. I. Day, *J. Org. Chem.*, 2012, **77**, 606–611.

22 L. H. Wu, X. L. Ni, F. Wu, Y. Q. Zhang, Q. J. Zhu, S. F. Xue and Z. Tao, *J. Mol. Struct.*, 2009, **920**(1–3), 183–188.

23 S. Y. Jon, N. Selvapalam, D. H. Oh, J. K. Kang, S. Y. Kim, Y. J. Jeon, J. W. Lee and K. Kim, *J. Am. Chem. Soc.*, 2003, **125**(34), 10186–10187.

24 H. Isobe, S. Sato and E. Nakamura, *Org. Lett.*, 2002, **4**(8), 1287–1289.

25 X. L. Ni, X. Xiao, H. Cong, Q. J. Zhu, S. F. Xue and Z. Tao, *Acc. Chem. Res.*, 2014, **47**, 1386–1395.

26 S. Sinn, A. Prabodh and L. Grimm, *Chem. Commun.*, 2020, **82**, DOI: 10.1039/d0cc03715j.

27 A. Sowa and J. Voskuhl, *Int. J. Pharm.*, 2020, **586**, 119595.

28 Q. Ai, L. Jin L and Z. Gong, *Chem. Soc. Rev.*, 2020, **18**, 10581–10585.

29 J. Murray, K. Kim, T. Ogoshi, W. Yao and B. C. Gibb, *Chem. Soc. Rev.*, 2017, **46**, 2479–2496.

30 J. Mosquera, Y. Zhao, H. Jang, N. Xie, C. Xu, N. A. Kotov and L. M. Liz-Marzán, *Adv. Funct. Mater.*, 2019, 190208.

31 X. L. Ni, X. Xiao, H. Cong, L. L. Liang, K. Chen, X. J. Cheng, N. N. Ji, Q. J. Zhu, S. F. Xue and Z. Tao, *Chem. Soc. Rev.*, 2013, **42**, 9480–9508.

32 J. Lü, J. X. Lin, M. N. Cao and R. Cao, *Coord. Chem. Rev.*, 2013, **257**, 1334–1356.

33 X. L. Ni, S. F. Xue, Z. Tao, Q. J. Zhu, L. F. Lindoy and G. Wei, *Coord. Chem. Rev.*, 2015, **287**, 89–113.

34 W. W. Zhao, L. T. Wie, K. Z. Zhou and P. H. Ma, *ChemistrySelect*, 2019, **4**(40), 11674–11677.

35 Y. X. Qu, K. Z. Zhou, K. Chen, Y. Q. Zhang, X. Xiao, Q. D. Zhou, Z. Tao, P. H. Ma and G. Wei, *Inorg. Chem.*, 2018, **57**, 7412–7419.

36 R. X. Cheng, F. Y. Tian and Y. Q. Zhang, *J. Mater. Sci.*, 2020, **55**, 16497–16509.

37 L. Mei, F. Z. Li, J. H. Lan, C. Z. Wang, C. Xu, H. Deng, Q. Y. Wu, K. Q. Hu, L. Wang, Z. F. Chai, J. Chen, J. K. Gibson and W. Q. Shi, *Nat. Commun.*, 2019, **10**, 1532.

38 M. H. Abraham and J. A. Platts, *J. Org. Chem.*, 2001, **66**(10), 3484–3491.

39 X. J. Cheng, L. L. Liang, K. Chen, N. N. Ji, X. Xiao, J. X. Zhang, Y. Q. Zhang, S. F. Xue, Q. J. Zhu, X. L. Ni and Z. Tao, *Angew. Chem., Int. Ed.*, 2013, **52**(28), 7252–7255.

40 Y. J. Zhao, S. F. Xue, Q. J. Zhu, Z. Tao, J. X. Zhang, Z. B. Wei, L. S. Long, M. L. Hu, H. P. Xiao and A. I. Day, *Chin. Sci. Bull.*, 2004, **49**, 1111.

41 G. M. Sheldrick, *Acta Crystallogr., Sect. A: Found. Crystallogr.*, 2008, **64**, 112–122.

42 X. D. Zhang, T. Sun and X. L. Ni, *Org. Chem. Front.*, 2021, **8**, 32–38.